TRIPLET-MATCHING FOR DEM GENERATION WITH PRISM, ALOS

---- A Case Study using Air-Borne Three Line Scanner Data

Tianen CHEN [*], Ryosuke SHIBASAKI [*], Koichi TSUNO [**], and Kazuya MORITA [**]

[*] Shibasaki Lab, Institute of Industrial Science, University of Tokyo
4-6-1 Komaba, Meguro-ku, Tokyo 153-8505, JAPAN
shiba@skl.iis.u-tokyo.ac.jp
[**] STARLABO Corporation
1-20-1, Sanshin BLDG, Shibuya, Shibuya-ku, Tokyo 150-0002, JAPAN
chentian@iis.u-tokyo.ac.jp

Commission III, WG III/2

KEY WORDS: PRISM/ALOS, Three-Line Scanner, Pyramid Image, Triplet Image Matching, DEM Generation

ABSTRACT:

For natural landscape, area-based matching can be successfully applied because the elevation is undulating rather gently. On the other hands, urban areas with the mixture of artificial structures such as buildings and natural landscape, where the elevation tends to have steeper changes, conventional area-based matching may not be successful. Many computer vision papers demonstrated matching methods based on features such as edge and regions extracted from images have much better performance for artificial structures. 2.5 m ground resolution of PRISM, however, may not be enough to extract detailed features enough to represent artificial structures. This may suggest the combination of area-based and feature-based matching approach can be more appropriate for ALOS PRISM data. This paper presents the results of experiments on the combination of the two approaches using simulated PRISM image generated from air-borne image sensor, TLS (Three Line Scanner).

1. INTRODUCTION

A number of space-borne scanner systems using solid-state linear array of detectors have been successfully in operation for stereoscopic mapping since SPOT-1 was launched in 1986. Different from SPOT-1 and SPOT-2 launched in 1990, which are collecting stereo images by side-looking push-broom mode and have certain disadvantages, for example different atmospheric conditions can prevail on different passes, thus degrading the stereo images, MOMS (Modular Optoelectronic Multispectral Stereo Scanner)-02/D2, MEOSS (Monocular Electro-Optical Stereo Scanner), HRSC (High Resolution Stereo Cameras) and IKONOS-I of SpaceImaging collect digital along-track stereoscopic imagery using a three-line camera (Ebner *et al*., 1991 and 1992; Fraser and Shao, 1996; Frisch *et al*., 1998; Ebner *et al*., 1999; Kornus *et al*., 2000).

PRISM (Figure 1) of ALOS to be launched in 2004 has three radiometers for Forward, Nadir and Backward viewing to collect along-track stereoscopic imagery at 2.5m ground resolution on 691.65km orbit altitude above equator for 1:25,000 mapping. Each radiometer has field of view with over 70km. Observation width is switched to 70km and 35km respectively in the Nadir viewing radiometer, and in the Forward and Backward viewing radiometer, it is 35km. When 70km observation mode of the Nadir is selected, only the observation data of the Backward radiometer can be acquired simultaneously. To correct distortion of observation views due to the Earth's rotation, even if satellite dose not carry out the yaw steering to correct it PRISM has an Earth rotation

correction function and obtains images by selecting automatically the best image extraction position according to the satellite position information provided from the satellite system. Table 1 lists its main characters.
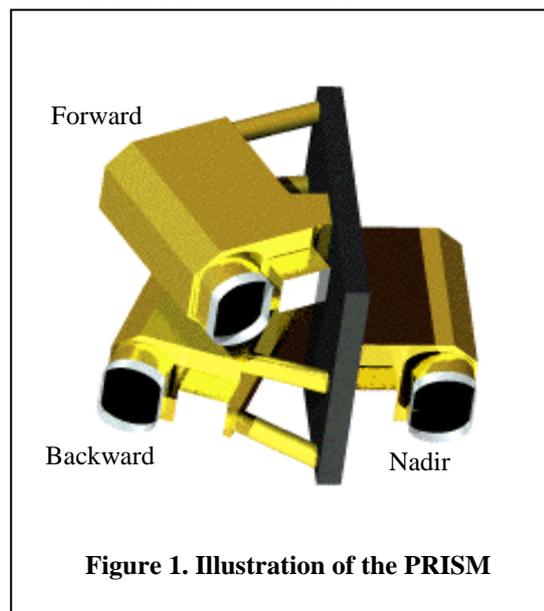
Figure 1. Illustration of the PRISM

This article deals with the extraction of height information from PRISM simulated imagery generated from SI-100 which is an airborne three-line-scanner developed by STARLABO Corporation jointly with University of Tokyo in 2000 (Chen *et al*., 2003). Table 2 lists the main characters of SI-100.

Item	Specification			Remarks
	Nadir	**Forward**	**Backward**	
Observation Band	0.52 to 0.77 μm			
IFOV	3.61 μrad			Converted distance on the ground surface: approx. 2.5 meters at the nadir
FOV	5.8 degrees.	2.63 degrees.		Max extraction width
Focal Length	1939mm	1939mm	1939mm	
Scan Cycle	0.37 millisecond ± 0.004 millisecond			
Pointing Angle	> ± 1.5 degrees.	> ± 1.36 degrees.		
MTF	> 0.2			Including MTF degradation along track by spacecraft flight
S/N	> 70			
Gain Setting	4 steps			It is possible to set per radiometer
B/H	-	1.0		
AD Bit	8			
Data Rate	< 960 Mbps (320 Mbps/telescope)			Before compression
Angle from nadir	± 23.8 degrees. (for forward and backward)			Along track
Side angle	-0.86 degree	-0.68 degree	0.86 degree	Perpendicular to track

Table 1 PRISM Main Characteristics

Item	Specification			Remarks
	Nadir	**Forward**	**Backward**	
Observation Band	RGB	RGB	RGB	
IFOV	0.0067 degrees.			Converted distance on the ground surface: approx. 10cm at the nadir
FOV	61.5 degrees.			Max extraction width
Focal Length	60mm			
Scan Cycle	0.002 second			
Flight Height	600 m			
AD Bit	12			
Data Rate	< 36 Mbps			
Angle from nadir	± 21.5 degrees. (for forward and backward)			Along track

Table 2 SI-100 Main Characteristics

This article deals with the extraction of height information from PRISM simulated imagery generated from SI-100 which is an airborne three-line-scanner developed by STARLABO Corporation jointly with University of Tokyo in 2000 (Chen *et al*., 2003). Table 2 lists the main characters of SI-100.

As conversional binocular aerial frame images for DEM generation, image matching methods are the key technique in DEM generation with PRISM imagery. Since there are no epipolar lines in PRISM stereo images and one-dimensional matching is unfeasible, an improved matching method using feature points and grids of PRISM imagery is proposed. The method has been developed by STARLABO Corporation jointly with University of Tokyo and successfully applied in SI-100 photogrammetry system. This paper briefly reviews the concept of the method and gives the DEM results with PRISM simulated images from SI-100. It also reports the accuracy by comparing with aerial images.

2. DESCRIPTION OF THE APPROACH

Figure 2 shows the concept of the algorithm for DEM generation with PRISM simulated imagery. In the following subsections we will describe these steps.

2.1 Preprocessing of the Image Data

According to the design specification of PRISM, each line sensor of PRISM is composed of several CCD line units collecting image segments for one image line in order to satisfy the high sampling frequency of image data. Each CCD unit generate one image strip. Certain overlap pixels between two neighboring CCD units ensure a whole image line for forward, nadir and backward view of PRISM. One task of preprocessing of PRISM image data is to merge the image strips generated by CCD units into a whole strip for PRISM forward, nadir, and backward viewing sensor.

The second task of preprocessing of PRISM image data is to extract the high precision orbit and attitude data from the recorded trailer data and interpolate these orientation data at

same sampling frequency of image data with the on-board GPS/IMU recording time so that each image line has its exterior orientation elements. Meanwhile, we will convert these exterior orientation elements into the mapping coordinate system such as UTM.

Figure 2. Concept of the algorithm for DEM generation with PRISM imagery
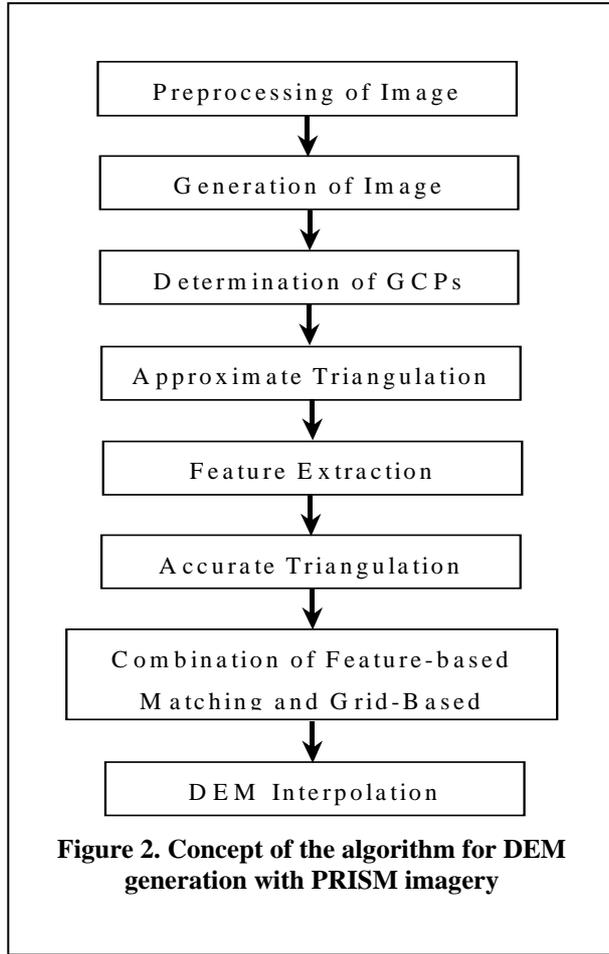
Also, the removal of stripping and the contrast enhancement should be performed with great care with respect to possible changes in the location of edges and other features.

2.2 Generation of Image Pyramids

As conventional aerial images, one scene of PRISM image corresponds to as much as several hundreds Megabytes data. For processing and managing this large amount of data efficiently, coarse-to-fine strategies based on image pyramids are at the very heart of every modern image matching algorithm. These strategies also further reduce the necessity for accurate initial values for the points to be matched. It was therefore straightforward to adopt a coarse-to-fine strategy for our approach. Figure 3 shows one example of generated image pyramids from PRISM simulated image.

2.3 Determination of Ground Control Points

Although on-board GSP/IMU can provide high precision orbit and attitude data for each PRISM image line, a certain number of ground control points are still necessary for removal of systematic errors such as offsets between GPS antenna and lens center, alignment between PRISM camera and IMU, and drift errors of IMU in later generalized bundle adjustment.

GCPs could be obtained through ground survey, aero triangulation, large scale existing vector maps and DEM. 2D (X, Y) or 1D (Z) can be used in our algorithm. It should be stressed, however, that the resulting absolute accuracy of the object point coordinates heavily depends on the quality and distribution of the control points.

2.4 Feature Extraction and Determination of Tie Points

Features in an image are distinct points, edges (or lines), and, areas. In our approach, we deal with point features only, because points can be used as tie points in triangulation and random points for DEM generation. In this subsection we only give one method to extract feature points from PRISM simulated images and the matching algorithm for extraction of tie points and random points for generating DEM.

2.4.1 Feature Extraction: Interest operators which locate point features in an image can be found in the literature (Förstner, 1986). Work on comparing these operators has shown that the Moravec and the Förstner operators perform best for real images in matching applications (Luhmann and Altrogge, 1986). The Förstner operator has some theoretical advantages compared to the classical Moravec operator (e.g., rotation invariance, and the potential for subpixel accuracy). We briefly describe the Förstner operator in following and select it in our approach.

The Förstner operator is based on the summary values of square gray value differences along the two diagonal directions over a window of specified size. Using these values we can calculate the rotation invariance and weight of the window center. Given a M×N window with center on $(i + M / 2, j + N / 2)$ in an image, the rotation invariance and weight of the window center are calculated as follows:

$$
\begin{cases}
V_x = \sum_{k=1}^{M-1}\sum_{l=1}^{N-1}[g(i+k+1, j+l+1) - g(i+k, j+l)]^2 \\
V_y = \sum_{k=1}^{M-1}\sum_{l=1}^{N-1}[g(i+k+1, j+l) - g(i+k, j+l+1)]^2 \\
V_{xy} = \sum_{k=1}^{M-1}\sum_{l=1}^{N-1}[g(i+k+1, j+l+1) - g(i+k, j+l)] \bullet \\
\qquad\qquad [g(i+k+1, j+l+1) - g(i+k, j+l+1)] \\
R = \dfrac{4(V_x V_y - V_{xy}^2)}{(V_x + V_y)^2} \\
W = \dfrac{V_x V_y - V_{xy}^2}{V_x + V_y}
\end{cases}
$$

where, R is the rotation invariance of the window center, and if the R is larger than certain value it is more possible to take the window center as an ideal feature point; W is the weight of the window center, and if the W obtains the highest value in an area on the image we take the pixel as feature point . R and W can be used to control the density of the extracted feature points from PRISM nadir image.

2.4.2 Feature Matching: We used a combined matching modules which are: (a) cross-correlation feature point matching based on region growing strategy, (b) grid point matching based on relaxation, (c) least square matching with or without geometric constraint, and (d) semi-automatic feature point matching. The grid matching

based on the relaxation matching technique is performed on a PRISM stereo pair combined with any two viewing direction of the three images. The important aspect of this relaxation matching that differs from other area-based single point matching is its compatible coefficient function and its smoothness constraint satisfaction procedure. With the smoothness constraint, poor texture areas in the image can be bridged assuming the terrain surface varies smoothly over the image area.

(a) Level 2

(b) Level 1
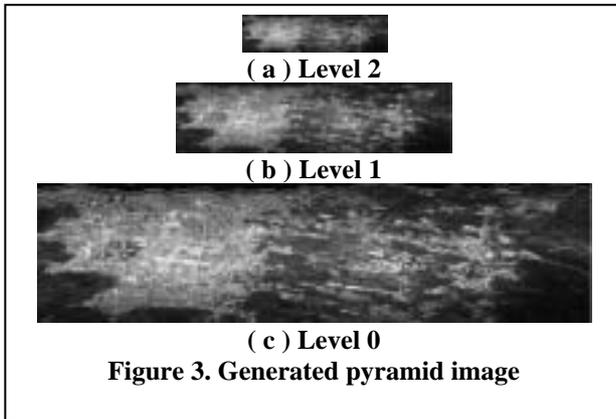
(c) Level 0
Figure 3. Generated pyramid image

Feature matching was firstly conducted on the highest pyramid level using the collinear equations with the approximate exterior orientation elements obtained from pre-triangulation based on a few GCPs. Meanwhile, a window tracking technique was used to pass the matched candidate points to the lower pyramid level for fine matching. Figure 4 shows the principle of our matching approach.
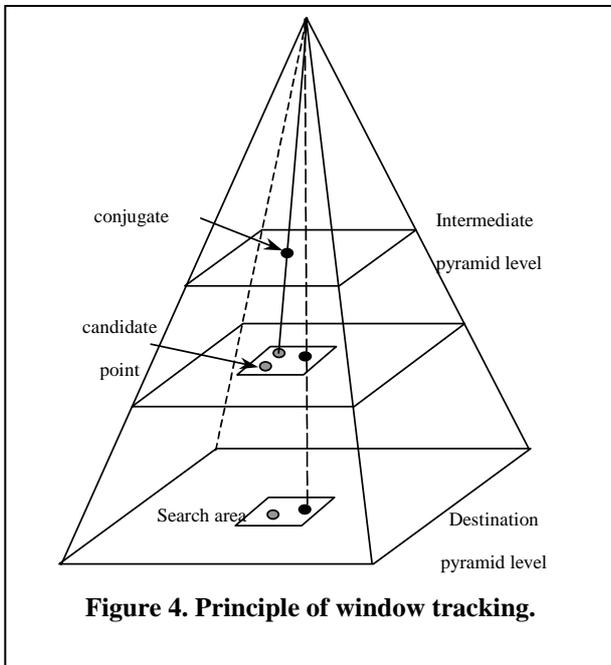
Figure 4. Principle of window tracking.

To find matches for the feature point, the epipolar geometric constrain in the forward and backward is used with the currently valid orientation parameters. All feature points within the search area are considered to be potential matches for the feature point in the nadir image. At the same time, we compute the conjugate point's ground mapping coordinates using

forward intersection through the combinations of Forward-Nadir, Forward-Backward, and Nadir-Backward. Only the combination whose computed ground mapping coordinates are the nearest is taken as the best match. The matched feature points will be verified in the next triangulation to check them intersect one point or not as Figure 5.
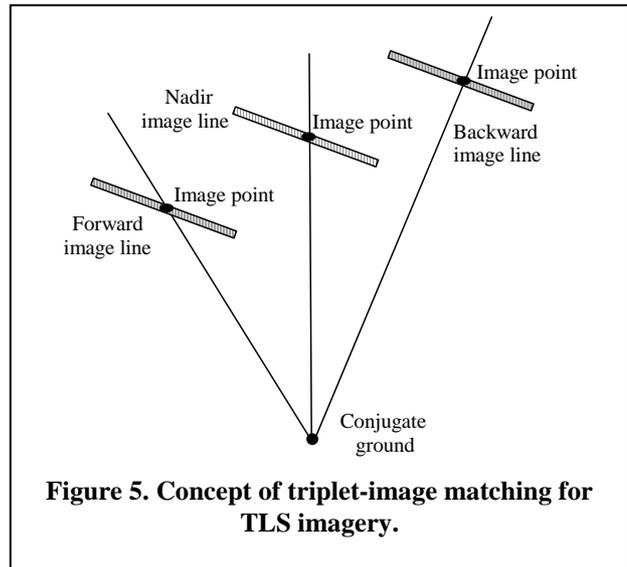
Figure 5. Concept of triplet-image matching for TLS imagery.

To increase the accuracy of image measurements of feature points, the least square image matching was used in the final step of our matching approach. Semi-auto image matching was used for user to select points in image where fewer points were matched. The extracted feature points were used as tie points in next triangulation to get more accurate exterior orientation correction values or used as seed points to extract more random points for DEM generation after the triangulation.

2.5 Generalized Bundle Adjustment

A number of research work and applications for the photogrammetric adjustment of 3-line-imagery have been conducted (Chen *et al.*, 2001; Lee *et al.*, 2000; Ebner et al., 1991 and 1992; Fraser and Shao, 1996; Frisch *et al.*, 1998; Ebner *et al.*, 1999; Kornus *et al.*, 2000). The DGR (Direct Geo-Reference) method was adopted in our approach since on-board high precision GPS/IMU data could be used for PRISM imagery orientation.
In the least square adjustment the GPS/IMU observation values as the approximate exterior orientation parameters, interior orientation parameters, ground control information and the image coordinates of the extracted conjugate points are considered as observations with corresponding standard deviations. From this information the unknowns (adjusted object point coordinates, adjusted offsets of GPS, alignments and drift errors of IMU) are derived. Additional unknowns are able to model a more camera motion.

2.6 DEM Generation

The generation of DEM involves the determination of conjugate points in the three image strips, the computation of object coordinates for these points and the interpolation of the object surface. To generating high accuracy DEM further information

such as single points and break lines should be also extracted by user manually.

Determination of conjugate points from PRISM three image strips is conducted with the above mentioned matching methods after the accurate orientation of these images have been determined so the search space can be much more limited, and the computation can be speeded up and the reliability of the matching results can be also increased. In this section we will briefly describe the combination of the feature point matching and grid point matching to get more density conjugate points for poor information areas in the images.

2.6.1   Grid point matching: Feature-based area matching always failed in poor information areas such as roofs of buildings, tops of trees, shadows of mountains and other objects in aero images and satellite images since no feature points could be extracted. Thus the disparity maps generated by the above matching algorithm contain some blank points without disparity values. To compensate these missed points, a grid point matching method is used here.
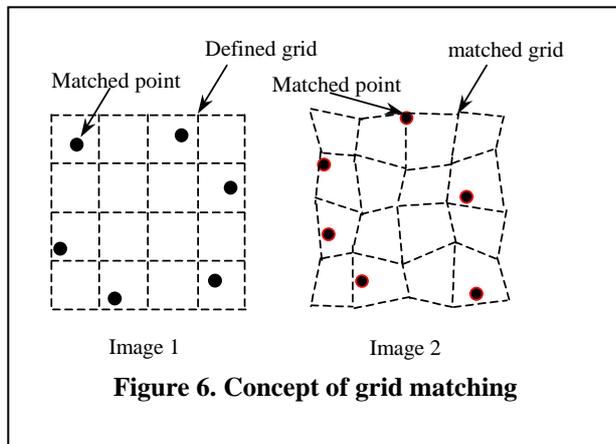
Figure 6. Concept of grid matching

Grid point matching belongs to multipoint matching method. It is based the matched feature points and tie points mentioned above. Figure 6 shows the concept. Assuming the poor information area a smooth surface and using the matched points around the poor information area to fit a mathematical function with least square method, we define a grid area for the poor information area by bilinear elements and get each grid point's gray value.

2.6.2   Combination of feature point matching and grid point matching: In this matching process we take the relaxation technique to reduce local ambiguity and achieve global consistency for grid points. More detail can be found in (Baltsavias, 1991; Zhang *et al*., 1992).

3.   EXPERIMENT RESULTS

One set of PRISM simulation data generated with SI-250 imagery in different areas was used to test our approach for DEM generation. The test images were taken with SI-250 at 600m flight height in Kesenuma area with size of 10km × 1km in 2003. The terrain surface covers a median-density residential area which lies in a hilly landscape with a local elevation difference of over 100 meters. Ground resolution of the obtained images was about 10cm. To coincide with PRISM imagery's ground resolution, we resampled the SI-250 images before the experiment. Figure 7 shows the resampled images. Total 9 GCPs were GPS-surveyed and converted into UTM coordinate system with standard deviation of 2cm for horizontal direction and 3cm for vertical direction. Only 5 GCPs were in the three overlap area of the simulated imagery. All GCPs were measured manually with our developed software. Additionally, several hundreds of pass points points were semi-automatically extracted from the three-overlap area. The accuracy of triangulation were about 25cm for horizontal and 30cm for vertical direction. Using the obtained triangulation results we generated DEM with our approach and compared with the DME generated from aerial images. Figure 8 shows the compared result.

(a) Forward view

(b) Nadir view
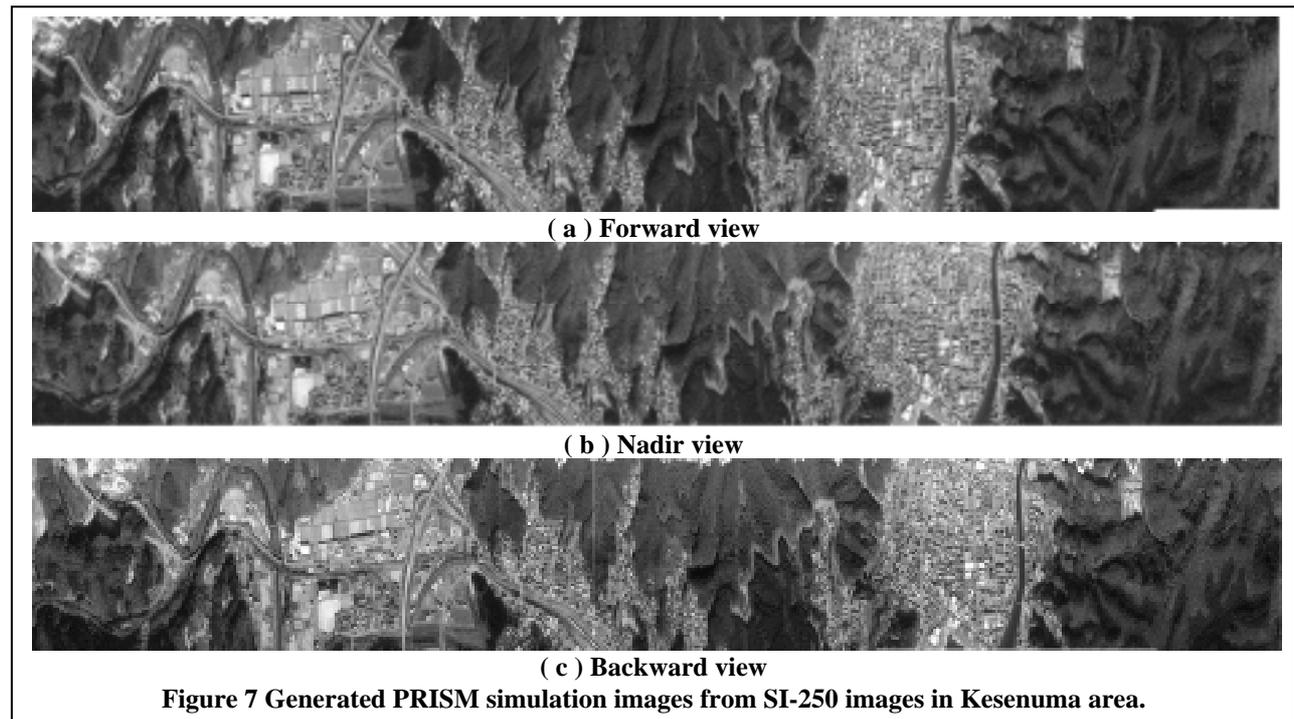
(c) Backward view
Figure 7 Generated PRISM simulation images from SI-250 images in Kesenuma area.

Figure 8. Differences between PRISM DEM and aerial image DEM in Kesennuma area.
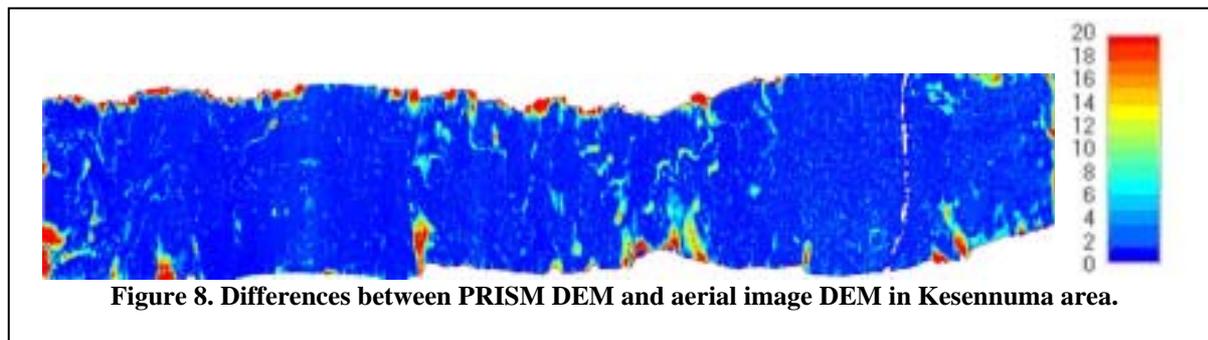
4. CONCLUSION

Two sets of PRISM simulation data generated from SI-250 were used to test out approach for DEM generation. We also compared the generated DEM from PRISM simulation data with the DEM generated from aerial images. The differences of more than 93% DEM grids are less than 3m. We have to point out that the interpolation methods of the two types of DEM are different. The difference between them was not counted here. From the triangulation results we think the accuracy can satisfy the requirement of DEM generation and line mapping with PRISM imagery. The combination of feature point-based matching and grid matching can be more appropriate for ALOS PRISM data. This paper presents the results of experiments on the combination of the two approaches using simulated PRISM image generated from air-borne image sensor, TLS (Three Line Scanner).

References:

Baltsavias, E.P., 1991. Multiphoto geometrically constrained matching. Ph.D. dissertation, Institute of Geodesy and Photogrammetry, ETH Zurich, Report No.49.

Chen T., R. Shibasaki, and K. Morita, 2001. High Precision Georeference for Airborne Three-Line Scanner (TLS) Imagery, 3rd International Imaging Sensing Seminar on New Developments in Digital Photogrammetry, Sept. 24-27, Gifu, Japan, pp. 71-82.

Chen T., R. Shibasaki, and S. Murai, 2003. Development and Calibration of the Airborne Three-Line Scanner (TLS) Imaging System, Photogrammetric Engineering & Remote Sensing, 69(1), pp.71-78.

Ebner, H. and G. Strunz, 1988. Combined Point Determination Using Digital Terrain Models as Control Information. Int. Arch. of Photogrammetry and Remote Sensing, Vol.27, Part B11, pp. III/578-587.

Ebner, H., W. Kornus and G. Strunz, 1991. A simulation study on point determination using MOMS-02/D2 imagery. Int. Journal of PE&RS, Vol.57 No.10, pp.1315-1320.

Ebner, H., W. Kornus and T. Ohlhof, 1992. A simulation study on point determination for the MOMS-02/D2 space project using an extracted functional model. Int. Arch. of Photogrammetry and Remote Sensing, Vol.29, Part B4, pp. 458-464.

Ebner, H., W. Kornus, T. Ohlhof, E. Putz, 1999. Orientation of MOMS-02/D2 and MOMS-2P/PRIRODA imagery. ISPRS Journal of Photogrammetry & Remote Sensing, Vol.54, pp. 332-341.

Förstner, W., 1986. A Feature Based Correspondence Algorithm for Image Matching. Proc. Int. Soc. for Photogr. and Remote Sensing, Symp. Comm. III, Vol.19.

Fraser, C. and J. Shao, 1996. Exterior orientation determination of MOMS-02 three-line imagery: Experiences with the Australian testfield area. Int. Arch. of Photogrammetry and Remote Sensing, Vol.XXXI, Part B3, pp. 207-214.

Fritsch, D., M. Kiefner, D. Stallman and M. Hahn, 1998. Improvement of the Automatic MOMS02-P DTM Reconstruction. Int. Arch. of Photogrammetry and Remote Sensing, Vol.32, Part B4, pp. 170-175.

Kornus W., M. Lehner, M. Schroeder, 2000. Geometric in-flight calibration of the stereoscopic line-CCD scanner MOMS-2P. ISPRS Journal of Photogrammetry & Remote Sensing, Vol.55, pp. 59-71.

Lee C., H.J. Theiss, J. S. Bethel, E. M. Mikhail, 2000. Rigorous Mathematical Modeling of Airborne Pushbroom Imaging System, Photogrammetric Engineering & Remote Sensing, 66(4), pp.385-392.

Luhmann, T., Altrogge, G., 1986. Interest Operators for Image Matching, Invited Paper, Symposium Comm. III, Rovaniemi.

Zhang Z., J. Zhang, X. Wu, and H. Zhang, 1992. Global image matching with relaxation method. Proc. International Colloquium on Photogrammetry, Remote Sensing and Geographic Information Systems, 11-14 May, Wuhan, China, pp.175-180.